Radiomic analysis of 3D spheroids using 2D brightfield images

Mariachiara Stellato [a,1] , Martyna Malgorzata Rydzyk [b,1] , Micaela Pannella [c] , Francesca Rossi [b] , Concettina Cappadone [b] , Daniel Remondini [a] , Jae-Chul Pyun [d] , Nicola Normanno [e] , Toni Ibrahim [c] , Gastone Castellani [f] , Emil Malucelli [b] , Stefano Iotti [b,g] , Enrico Lucarelli [c,*] , Filippo Piccinini [e,f]

[a] Department of Physics and Astronomy "Augusto Righi" (DIFA), University of Bologna, Bologna, Italy
[b] Department of Pharmacy and Biotechnology (FABIT), University of Bologna, Italy
[c] Osteoncology, Bone and Soft Tissue Sarcomas and Innovative Therapies Unit, IRCCS Istituto Ortopedico Rizzoli (IOR), Bologna, Italy
[d] Department of Materials Science and Engineering, Yonsei University, Seoul, Republic of Korea
[e] IRCCS Istituto Romagnolo per lo Studio dei Tumori (IRST) "Dino Amadori", Meldola, FC, Italy
[f] Department of Medical and Surgical Sciences (DIMEC), University of Bologna, Bologna, Italy
[g] National Institute of Biostructures and Biosystems, Rome, Italy

ARTICLE INFO

ABSTRACT

Background and Objective: Radiomics is a field of quantitative imaging involving the extraction of features from medical images transforming them into mineable data for diagnostic, prognostic, and predictive purposes. In this work, we focused on the analysis of 2D brightfield images acquired with standard microscopes today available in all biological laboratories.
Methods: We analysed images of 3D multicellular spheroids, an *in vitro* model commonly used in Regenerative Medicine and Oncology. Besides describing *Analysis of Spheroid* version 3.0 (*AnaSP 3.0*), a new release of an open-source software suite specifically designed for segmenting and extracting features from 2D brightfield spheroid images. To validate the tool, spheroids generated with U-shape bottom multi-well plates and different concentrations of mesenchymal stem cells and osteosarcoma cell lines have been used.
Results: We demonstrated how advanced features included in *AnaSP 3.0*, *i.e.* sphericity, volume, and image gradient, may be used to indirectly assess the spheroidization of the spheroids over time, the number of cells composing the spheroids, and the extension of a possible central necrotic core.
Conclusions: AnaSP 3.0 is freely available at https://sourceforge.net/p/anasp. Compared to the previous versions, it includes a new algorithm for volume estimation and introduces new modules to extract advanced features using the original grey-level image values, rather than just relying on binary masks.

1. Introduction

Today, three-dimensional (3D) *in vitro* models are extremely popular [1]. They have a predominance of cell–cell interactions over cell-substrate interactions, better mimicking histo-morphological, functional, and environmental characteristics of *in vivo* tumour tissues (*i. e.*, spatial organisation, extracellular matrix (ECM) deposition, and gradients of oxygen, nutrients, and signalling molecules). The use of 3D cell cultures dates back to the early 20th century when researchers recognised the limitations of traditional two-dimensional (2D)

monolayer cultures in mimicking the complexity of tissues and organs. However, spheroids started gaining significant attention as an *in vitro* model only in the 1970 s [2]. Nowadays, spheroids are substituting 2D cell cultures in several fields, including oncology and regenerative medicine. In oncology, 3D multicellular spheroids are widely used for testing drugs and studying the effect of radiotherapy treatments [3]; in regenerative medicine, they are mainly used for building new tissues and repairing damaged ones [4].

Spheroids can be used to retrieve various types of quantitative data. Genetic, histological, and multi-omic data are typically extracted and analysed, but microscopy images can be the greatest source of information. Different methods are employed for acquiring the images of the spheroids. Among them, one of the most common is brightfield microscopy [5]. This is a fundamental technique in the realm of light microscopy, providing straightforward and accessible means to observe a variety of specimens, such as spheroids. Its simplicity, reliability, and ability to visualise intricate details have made it an indispensable tool for scientists across diverse disciplines. Its direct and unmanipulated view of the sample, allows the observation of live cells, microorganisms, and a wide range of biological materials. Its ability to reveal cellular morphology, subcellular structures, and intricate patterns makes it invaluable for studying cell division, tissue organisation, and pathological processes. The simplicity and cost-effectiveness of brightfield microscopy have made it a ubiquitous tool in laboratories worldwide [6]. Other microscopy techniques can be used for analysing spheroids, such as phase-contrast, differential interference contrast (DIC), widefield fluorescence, confocal, and light sheet (the last three requiring fluorescence staining) [7].

It is possible to extract quantitative features and analyse them to provide valuable information for diagnosis, prognosis, and assessment of treatment response starting from brightfield images. The field of study that is centred around data extraction from images is called radiomics. It involves the application of advanced image processing techniques, machine learning, and statistical modelling to extract and analyse a large number of features from medical images. Radiomics is based on the principle that medical images contain more information than what is visible to the naked eye. These images capture detailed spatial and textural patterns that can be quantified and analysed to reveal insights about underlying tissue characteristics, tumour heterogeneity, and disease progression. Radiomics leverages pixel- or voxel-level intensity values, as well as spatial relationships and texture patterns, to derive meaningful and reproducible features [8].

During the last few years, several tools have been developed to perform radiomic analysis of different types of images. For instance, *AMIDA* [9], *Analysis of Spheroid (AnaSP)* [5], *INSIDIA* [10], *PCaAnalyser* [11], *SpheroidJ* [12], *SpheroidSizer* [13], and *TASI* [14] are freely available tools for extracting morphological features of spheroids. Among them, *AnaSP* is a freely available open-source tool that was conceived to provide a comprehensive and easy environment composed of various modules to extract radiomic features and was used to estimate Radiomic features in several different conditions [1]. In this work, besides describing *AnaSP* 3.0, a new release including grey-level features, we tested the tool using spheroids generated with U-shape bottom 96 ultra-low attachment multi-well plates and different concentrations of cell lines. The spheroidization over time, the number of cells composing the aggregate, and the extension of the necrotic core were indirectly assessed. using sphericity, volume, and grey-level gradient (the latter defined as the linear change of image brightness's intensity along a specific direction).

It is worthy to underline that some cell lines used to generate spheroids, including osteosarcoma cancer cells, cannot grow as 3D aggregates with spherical symmetry [1,15]. On the other hand, when the same tumoral cells are mixed with mesenchymal stromal cells (or mesenchymal stem cells, MSCs), the aggregates obtained have a higher spherical symmetry degree. To quantify the degree of sphericity, different lines of spheroid were created, each with a different

concentration of cancer and MSCs. Using the radiomics data obtained with the last version of *AnaSP* (*i.e.* 3.0), it was possible to characterise the sphericity of the different spheroids, in correlation with the mixture of cells composing them.

One of the most common quantitative data extracted from a 3D spheroid is the total number of cells [16]. This operation is typically done by disaggregating the spheroid and using counting chambers to estimate the total number of cells under microscope or automated cell counters [17]. This is a complicated task requiring the destruction of the spheroid, meaning that no further analysis is possible. To avoid this problem, a new feature was implemented in *AnaSP* 3.0 that estimates the number of cells composing the spheroid. It requires as prior a brightfield image and the average volume of a single composing cell. The implemented feature was validated by analysing various osteosarcoma spheroids both with the computational tool and by disaggregating them to determine the ground truth values.

Finally, one of the main challenges of spheroid analysis is determining the presence of a necrotic core, typically defined as a central region of the spheroid where cells undergo necrosis due to lack of oxygen and nutrients [18]. Various methods can be employed to extract information from the necrotic part of the spheroids, such as fluorescence staining and slicing. However, these methods damage the constructs functionally and structurally, not allowing further analysis. Starting from the analysis of the average and local grey level values, we have developed a feature that allows the user to study the presence, and even the extent of the necrotic core of a spheroid without destroying its structure.

2. Materials and methods

2.1. AnaSP 3.0

AnaSP is an open-source tool to perform radiomics analysis of 3D multicellular spheroid starting from 2D images (Fig. 1A). Its first release (*i.e.* version 1.0) dated to 2015 [5]. Up until *AnaSP* 2.0 (released in 2023), the radiomic features implemented were extracted only from the binary masks without considering original intensity values [19]. Namely, only morphological features could be computed (Fig. 1B): (*1*) Area, (*2*) Circularity, (*3*) Compactness, (*4*) Convexity, (*5*) Equivalent Diameter, (*6*) Minor Diameter Through Centroid, (*7*) Feret Aspect Ratio, (*8*) Maximum Diameter Through Centroid, (*9*) Feret Maximum Diameter, (*10*) Feret Minor Diameter, (*11*) Feret Maximum Diameter Orthogonal Distance, (*12*) Perimeter, (*13*) Sphericity, (*14*) Solidity, (*15*) Volume. In the new version of the tool, *AnaSP* 3.0, a new group of features was implemented to recover information from the segmentation and the brightness of the original brightfield images (converted in 8-bit grey-level images in case of RGB or different formats, Fig. 1C): (*I*) Average Grey-Level, (*II*) Cell Number, (*III*) Entropy, (*IV*) Kurtosis, (*V*) Necrotic Percentage, (*VI*) Skewness, (*VII*) Standard Deviation. All the mathematical details of the different features are reported in the *AnaSP*'s User Manual (distributed together with the source code and standalone versions of the tool). *AnaSP* 3.0 was also integrated with another open-source tool, *ReViSP* [20,2], able to create 3D renderings of the spheroids starting from the 2D binary masks. The new options of the software have been implemented in a second window (Fig. 1A, right side). The *AnaSP* 3.0 source code, standalone applications for MAC, and Windows, video tutorials, manual documentation, and sample datasets are publicly available at: *https://sourceforge.net/p/anasp*.

2.2. Sphericity, cell number, necrotic percentage

Among the 22 features currently implemented in *AnaSP*, 3 are specifically discussed in this work: sphericity, cell number, and necrotic percentage. (*a*) Sphericity (S), a binary feature that aims to estimate how far the shape of the object in the image is from a sphere. Sphericity is calculated as reported in [21] (Eq. (1):

A

B
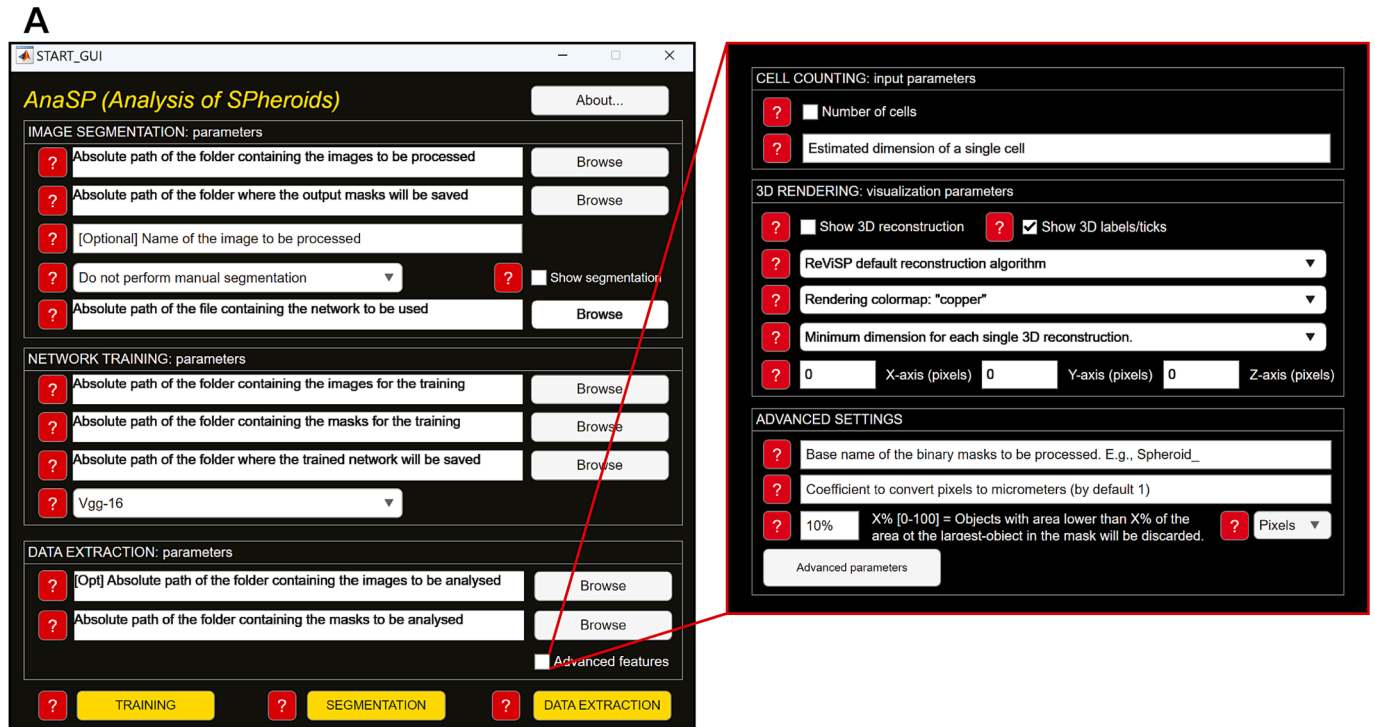
Binary Morphological Features

Area	Circularity	Compactness	Convexity	Equivalent Diam.
Min. Diam. Through Centroid	Feret Aspect Ratio	Max. Diam. Through Centroid	Feret Max. Diam.	Feret Min. Diam.
Feret Max. Diam. Orthogonal Distance	Perimeter	Sphericity	Solidity	Volume

C

Grey-level Features

Average Grey-Level	Standard Deviation	Entropy	Skewness	Kurtosis	Cell Number	Necrotic Percentage

Fig. 1. *AnaSP 3.0* scheme. (**A**) *AnaSP 3.0* main and secondary window. (**B**) Binary morphological and (**C**) grey-level features implemented in *AnaSP 3.0*.

$$S = \frac{\pi\sqrt{4\frac{Area}{\pi}}}{Perimeter} \tag{1}$$

Area is the area in pixels of the foreground; *Perimeter* is the length in pixels of the perimeter of it. *S* is a dimensionless number ranging from *0 to 1*, where *1* indicates a perfect circle. (*b*) Cell Number, to estimate the number of cells contained in a spheroid, specifically in a monoculture setup and without a necrotic core. If a necrotic core is present, the assumption that the volume of individual cells remain constant no longer holds. To extract this feature (*I*) the original grey-level image, (*II*) the binary mask, (*III*) the average volume of a single cell, and (*IV*) the conversion factor to convert from pixels in the unit of measure (*e.g.* micrometres), have to be provided as input. Cell Number is computed by dividing the volume of the spheroid (estimated using the integrated *ReViSP* algorithm) by the average volume of a single cell. (*c*) Necrotic Percentage, a feature that aims to determine the percentage of necrosis in the spheroid (if present). To perform this calculation, the software needs only the original image and the relative binary mask. After a series of morphological operations, the intensity of the image brightness gradient is analysed to estimate the area where the necrotic region starts and the Necrotic Percentage is finally calculated by computing the ratio with the total spheroid area. This is possible because, in the necrotic region, the density of the nuclei changes with respect to the proliferating and quiescent regions, leading to inhomogeneity in the gradient values. For this reason, this method should be exclusively used for monoculture spheroids because changes in density might arise from cell-type differences rather than necrosis, making reliable interpretation challenging.

2.3. Cell lines

Three different cell types were used for the experiments: (*a*) Saos-2 is a cell line composed of cells with epithelial morphology isolated from the bone of an 11-year-old, white, female osteosarcoma patient (ATCC, Manassas, VA, USA). The cell line expansion was conducted under normoxic conditions in Mc Coy's medium (Life Technologies-Thermo Fisher Scientific, Waltham, MA USA) supplemented with 15 % fetal bovine serum (FBS, Thermo Fisher Scientific, Massachusetts, USA), 1 % Gibco™GlutaMAX™ supplement (Thermo Fisher Scientific, Massachusetts, USA) and 1 % of Penicillin-Streptomycin antibiotic (Thermo Fisher Scientific, Massachusetts, USA), was changed twice weekly. (*b*) Human Mesenchymal Stem Cells (MSCs) were obtained from bone marrow samples of patients undergoing surgery at Rizzoli Orthopedic Institute (IOR, Bologna, Italy) after patients' informed consent, according to the protocol approved by the local ethical committee (n. 0029817/2015). Withdrawal of bone marrow from the posterior iliac crest and gradient separation of mononucleated cells with Ficoll®-Paque PREMIUM 1.073 (GE Healthcare Life Sciences, Uppsala, Sweden) were performed following an established protocol [22]. Mononuclear cells were then seeded in cell culture flasks (Corning, Glendale, Arizona, USA) in complete growth medium MEM alpha medium (Euroclone S.p.a., Milan, Italy), completed with 20 % of FBS, 1 % of Gibco™ GlutaMAX™ supplement (Thermo Fisher Scientific, Massachusetts, USA), and 1 % of Penicillin-Streptomycin antibiotic at a density of 4×10^5 cells/cm2 and incubated at 37 °C in 5 % CO2 atmosphere, changing medium twice a week up to 70 % confluency. After the first passage sub-culturing was performed at 2×10^3 cell/cm². At passage 3 isolated MSCs were

characterised in terms of Fibroblast-Colony Forming Unit (CFU-F) efficiency, immunophenotypic profile, proliferation rate, and trilineage-differentiation potential [23 24]. (*c*) 143B is a cell line isolated from the bone of a 13-year-old, white female human with osteosarcoma (ATCC, Manassas, VA, USA). The 143B cells were cultured in Dulbecco's Modified Eagle's Medium (Life Technologies-Thermo Fisher Scientific, Waltham, MA USA) supplemented with 10 % FBS, 1 % of Gibco™ GlutaMAX™ supplement and 1 % of Penicillin-Streptomycin antibiotic.

2.4. Microscopes

Three different types of microscopes were used: (*a*) For performing time-lapse acquisition of brightfield images, an automatic IncuCyte S3 (Sartorius, Göttingen, Germany) system embedded with a 10 × magnification objective was used. The final image size was fixed at 1408 × 1040 pixel resolution, and the images were saved as ".tif" (RGB, 8-bit/channel). (*b*) A Nikon (Tokyo, Japan) Eclipse TE2000-U inverted microscope, equipped with a Nikon CMOS USB 3.0 10MP Camera, was used for specific time-point brightfield images. The parameters were chosen at the beginning of the acquisition to have the best possible contrast and completely exploit the grey levels range. The exposure was 8 ms, with a gain equal to one. The "auto white" setting was exploited to have three colour channels aligned with the peak of the grey-level histogram. A 20 × and 10 × magnification factors were selected to acquire the images. The final image size was fixed at 1200 × 1600 pixel resolution, and the images were saved as ".tiff" (RGB, 8-bit/channel). Each acquired image was then converted to grayscale using ImageJ, a well-known open-source image processing software [25]. (*c*) To acquire fluorescent images of the single cells, a confocal Nikon D-eclipse C1 laser scanning confocal microscope system-SHV C1-DUT, composed of a Nikon Eclipse E600 microscope and 3 laser diode modules (405/488/543 nm), was used. Its scanning head has 3 photomultiplier tubes (PMTs) which can detect simultaneous 3-channel fluorescence in double- and triple-labelling experiments. A 40 × magnification factor was used to acquire the single-cell images. The final image size was fixed at 512 × 512 pixel resolution and the images were saved as ".tif" (RGB, 8-bit/channel). All the images acquired in the experiments are freely reported as Supplementary Materials available at *https://doi. org/10.6084/m9.figshare.c.7253371*.
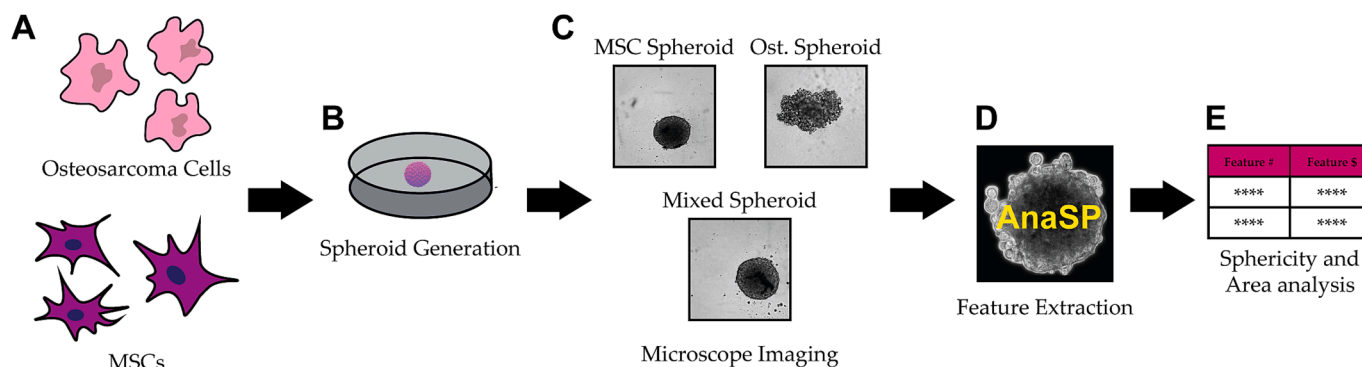
2.5. Spheroidisation

The first experiment aimed to study how the presence of MSCs can influence the sphericity of osteosarcoma spheroids. We generated spheroids using the Saos-2 cell line and MSCs cells (Fig. 2A). Five different spheroid conditions were generated, with different ratios of the two cell lines: 0 % MSCs and 100 % Saos-2; 25 % MSCs and 75 % Saos-2; 50 % MSCs and 50 % Saos-2; 75 % MSCs and 25 % Saos-2; 100 % MSCs

and 0 % Saos-2 (Fig. 2B). In each experimental condition, 48 spheroids were seeded into individual wells of a 96-well ultra-low-attachment plate. The seeding density employed was 5000 cells per well. The growth medium for each condition was prepared by mixing the medium of the different cell lines according to the specific cell percentages. After the seeding, the cells were centrifuged for 3 m. Then the plate was incubated at 37 °C, 5 % carbon dioxide, and 95 % humidity in IncuCyte S3 facilities, and the spheroid growth was monitored for 5 days. This microscope can automatically acquire time-lapse images, and it was used to acquire images every 6 h over five days, meaning 21 acquisitions for each spheroid (Fig. 2C). The microscope was coupled with the homonym software, able to segment the spheroids and perform statistical analysis. Starting from the binary masks obtained, area and sphericity were calculated using *AnaSP* (Fig. 2D and E). Original images and masks related to co-culture spheroids analysed over time are available as Supplementary Material 1. Propidium Iodide (PI, Fluka ® Milan, Italy) staining of the spheroids was performed at the endpoint. PI is a popular red-fluorescent nuclear and chromosome counterstain. Since PI is not permeant to live cells, it is used to detect dead cells in a population. The PI solution was prepared at 1 mg/mL concentration in DMSO (Sigma-Aldrich St. Louise, MO, USA) and used at the concentration of 5 μg/mL. To visualise the entire spheroid in fluorescence, all nuclei were stained with Hoechst 33,342 (Sigma-Aldrich St. Louise, MO, USA). After 30 m incubation, the spheroids were observed under a confocal microscope using a 10 × magnification factor. To confirm the results obtained with the PI assay, the resazurin assay, a metabolic assay, was performed. Briefly, 50 μL of fresh medium and 20 μL of Resazurin (TCI, Milan, Italy) at the concentration of 600 μM was added to each well. The plate was then incubated overnight at 37 °C, 5 % carbon dioxide, and 95 % humidity. The next day the medium was collected and the fluorescence signal was measured with a plate reader (EnSight Multimode Plate Reader, Milano, Italy) applying a ʎ excitation of 560 ηm and ʎ emission of 590 ηm. Finally, the data was determined by subtracting the background signal from the individual spheroid data and calculating the average per condition. The images obtained with the confocal microscope (10x magnification factor, with a 1.7 μm/pixel conversion coefficient) for the PI and Hoechst stainings are available as Supplementary Material 2.

2.6. Cell number

The second experiment, concerning the estimation of the number of cells in the spheroid using a single brightfield image, was performed through the following steps: (*a*) spheroid generation (Fig. 3A and B); (*b*) brightfield image acquisition (Fig. 3F); (*c*) spheroid disaggregation (Fig. 3C) to count the number of cells using standard technologies (Fig. 3D and E); (*d*) single-cell volume estimation using a confocal microscope.

Fig. 2. Scheme of the spheroidisation experiment. (**A**) Cartoon of the MSC and osteosarcoma cell lines. (**B**) Co-culture spheroid generation, with various mixtures of the two cell lines. (**C**) Examples of brightfield images of spheroids acquired with the IncuCyte microscope. Approximate diameter of the spheroids: 300–700 μm. (**D**) Feature extraction performed with *AnaSP*. (**E**) Schematic representation of the features analysed over time.
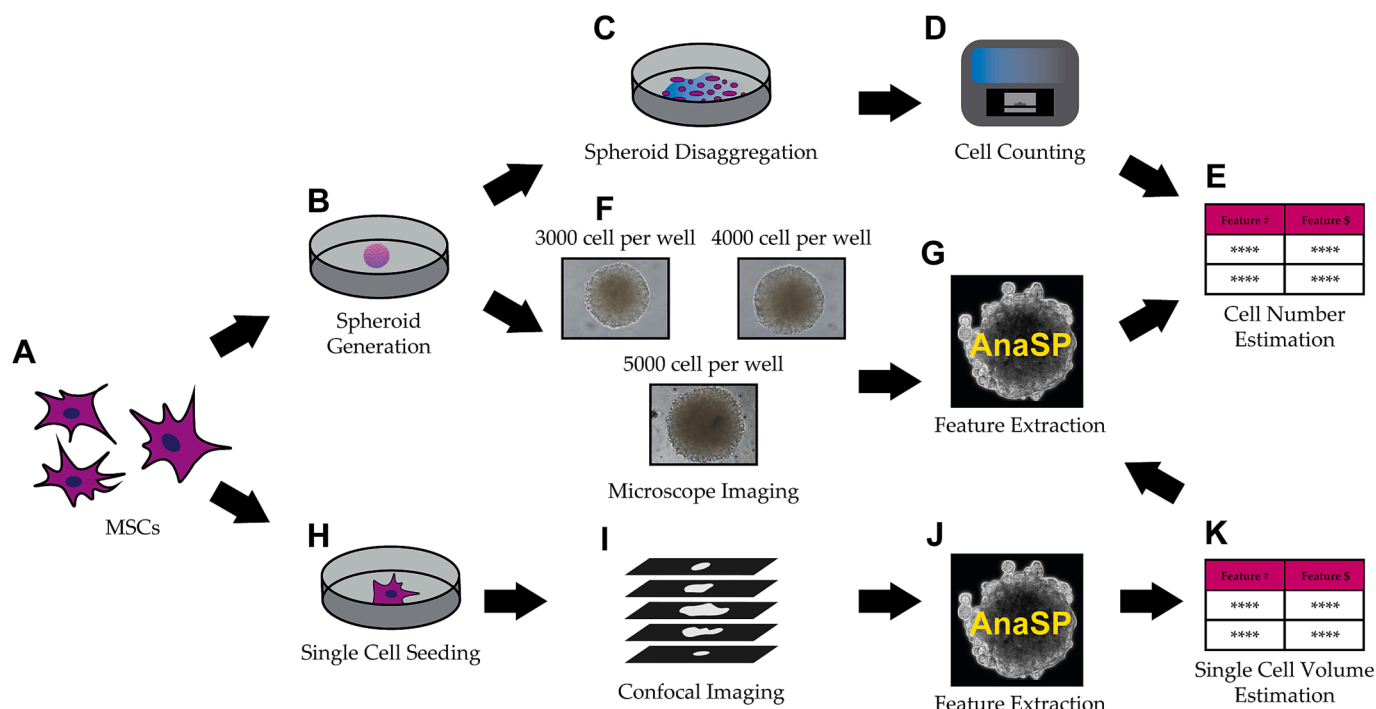
Fig. 3. Scheme of the cell number experiment. (**A**) Cartoon of the MSCs. (**B**) Generation of monoculture spheroids. (**C, D**) Representation of the process for the evaluation of the number of cells based on a classical cell counting approach. (**C**) Cartoon of the spheroid disaggregation obtained through an enzymatic dissociation. (**D**) Cartoon of the cell counting through a hardware device. (**E**) Schematic representation of a table reporting the extracted features, in particular the number of cells. (**F, G**) Representation of the process for the evaluation of the number of cells using *AnaSP*. (**F**) Examples of brightfield images of spheroids acquired with a brightfield microscope. Approximate diameter of the spheroids: 300–350 μm. (**G**) Feature extraction performed with *AnaSP* for cell number estimation. (**H, I, J, K**) Representation of the process for the evaluation of the average volume of the single cells. (**H**) Seeding of single cells. (**I**) Schematic representation of 3D single-cell images acquired with a confocal microscope. (**J**) Feature extraction performed with *AnaSP* for the single-cell volume estimation. (**K**) Schematic representation of a table reporting the extracted features, in particular the volume of the single cells.

The spheroids were created starting from the MSCs only (Fig. 3A). The cells were seeded in 96-well ultra-low-attachment plates (Corning Inc., Kennebunk (ME), USA, Fig. 3B). Three different cell densities were seeded: 3000, 4000, and 5000 cells per well, in 100 μL of MEM alpha medium (Euroclone S.p.a., Milan, Italy), supplemented with 20 % of FBS, 1 % of Gibco™ GlutaMAX™ supplement (Thermo Fisher Scientific, Massachusetts, USA), and 1 % of Penicillin-Streptomycin antibiotic. An equal number of spheroids for each seeding density was generated,

meaning 32 spheroids per type. After 48 h of incubation at 37 °C, 5 % carbon dioxide, and 95 % humidity, the images were acquired with the Nikon Eclipse TE2000-U inverted microscope (Fig. 4B). The spheroids were imaged after 48 h to limit the formation of the necrotic core. The segmentation binary masks and volume 3D rendering used to compute the volume were obtained with the manual segmentation feature provided by *AnaSP* (Fig. 4C and D). The substrate was then removed and washed twice with a phosphate-buffered saline (PBS) solution to
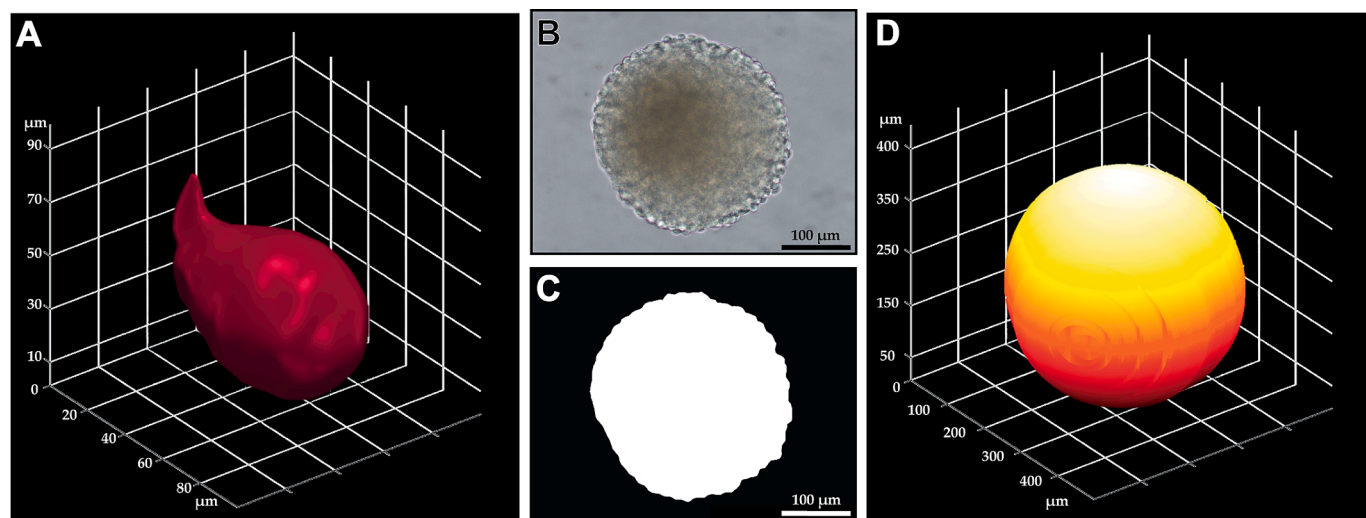

Fig. 4. Representation of the volumes used for the cell counting. (**A**) 3D rendering of the volume of a single MSC. (**B**) Brightfield image of a spheroid generated with a 3000 cell/well density. (**C**) Binary mask of (**B**). (**D**) 3D rendering of the volume of the spheroid in (**B**). The binary mask (**C**) and the 3D rendering (**D**) have been generated with *AnaSP*.

eliminate the medium. The PBS was then replaced with 50 µL per well of the disaggregation solution (Fig. 3C), composed of Gibco™ TrypLE™ Express Enzyme (1X), without phenol red mixed with 0.2 mg/mL of Gibco™ Collagenase, Type I, powder. After 1 h, the spheroids were separated using a pipette (CLEARLine® Filter tips racked sterile, Biosigma S.p.A., Verona, Italy) 10 times for each spheroid. The spheroids were incubated during the disaggregation period in a Thermolyne Vari-Mix™ Platform Mixer at 37 °C with 5 % of CO_2. After 45 min, the solution was resuspended 10 times with a pipette, for a total disaggregation time of 105 min. For every disaggregated spheroid, 10 µL of solution is withdrawn to perform the counting. Vital exclusion staining of mono dispersed cells culture was performed using erythrosine (Sigma-Aldrich, St. Louise, MO − USA) to distinguish the live cells. The protocol used entailed a mixture of 0.1 % erythrosine powder in a PBS solution. Erythrosine solution was added to cell dispersion in a ratio of 1:1, immediately after which the cell count was determined by the cell counter (Countess® II FL Automated Cell Counter, Fig. 3D). The number reported by the cell counter is the number of cells per µL, meaning that to obtain the total number of cells composing the spheroids, the result of the cell counter is multiplied by 20. For the second part of the experiment single cells (Fig. 3H) were stained with 1,1′-Dioctadecyl-3,3,3′,3′-tetramethylindocarbocyanine perchlorate − 97 % (DIL, Merck KGaA, Darmstadt, Germany) in MEM alpha medium without FBS in order to visualise the cells in fluorescence with the confocal microscope. The DIL was prepared with a concentration of 1 mM in EtOH absolute and applied at the dilution of 5 µL/mL. The cells were then washed and resuspended in a complete MEM alpha medium. To 200 µL of the 5×10^5 cells/mL cell suspension, 200 µL of Corning® Matrigel®Basement Membrane Matrix for 3D In Vitro Culture was added. The suspension was then seeded in an 8-well cell culture chamber (SARSTEDT AG & Co. KG Sarstedtstraße 1 51,588 Nümbrecht Germany). After 4 h the cells were observed under a confocal microscope using a 40 × magnification factor (Fig. 3I). Several stacks of images were obtained along the z axes, with an interslice distance of 0.7 µm. The obtained data were preprocessed using ImageJ. The red channel colour was selected, to retain the information about the cells. The image stack was converted into a sequence of images and these were finally converted into the 8-bit format. From the various cells contained in each stack, only the ones completely included in the stack, from top to bottom, were selected to perform the volume estimation. The volume estimation (Fig. 3 and K) was finally done with the *ReViMS* software (Fig. 4A) [26]. Finally, the estimation of the number of cells per spheroid was computed with *AnaSP 3.0* (Fig. 3G). The images and masks of MSC spheroids analysed with a brightfield microscope (20x magnification factor, 0.297 µm/pixel conversion coefficient) and mesenchymal stem single-cells analysed with a confocal microscope (40x magnification factor, 0.62 conversion coefficient) are available as Supplementary Material 3.

2.7. Necrotic core

The third experiment regards the estimation of the extension of the necrotic core in a monoculture spheroid (Fig. 5A and B) using only a 2D brightfield image (Fig. 5C). This approach differs from traditional methods that require 3D image stacks, typically acquired through techniques like light-sheet fluorescence microscopy, to perform similar analysis [27]. *AnaSP* is able to delineate a region where the density of the spheroid changes rapidly, deemed the necrotic region, by removing the background and estimate the intensity of the image brightness gradient only to the spheroid pixels (Fig. 5D). This value is used to extract the necrotic percentage feature as the ratio between the necrotic region and the total spheroid area (Fig. 5E). The protocol involves four steps: (*a*) spheroid formation and culture; (*b*) bright-field imaging; (*c*) fixation, embedding and staining; (*d*) histological slice imaging; (*d*) detection of the necrotic core. The spheroids were seeded from the 143B cell line in 96-well ultra-low-attachment plates (Corning Inc., Kennebunk, ME, USA). Three different spheroid densities were seeded: 5000, 7500, and 10,000 cells per well in 100 µL of Dulbecco's Modified Eagle Medium (DMEM) meaning 32 spheroids per type. Spheroids were incubated for 7 days at 37 °C, 5 % carbon dioxide, and 95 % humidity. The medium was changed once. After 7 days the substrate was removed and the samples were washed with a Phosphate-buffered saline (PBS). Brightfield images were acquired using the Nikon Eclipse TE2000-U microscope previously described. In particular, to acquire these images, it was fundamental to set (*I*) a high magnification factor for having
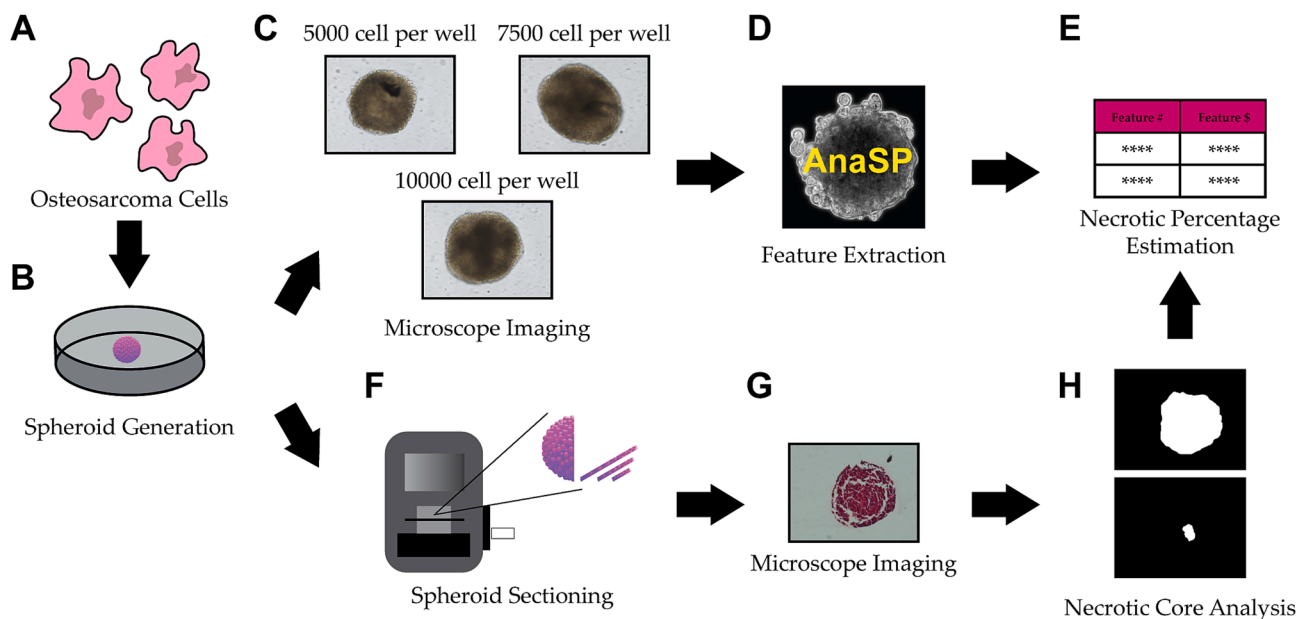
Fig. 5. Experiment scheme of the estimation of the necrotic core percentage. (**A**) Cartoon of the 143B osteosarcoma cells. (**B**) Generation of monoculture spheroids. (**C, D**) Representation of the process based on the gradient analysis of brightfield images. (**C**) Brightfield images of spheroids generated with three different cell seedings. Approximate diameter of the spheroids: 400–600 µm. (**D**) Feature extraction performed with *AnaSP*. (**E**) Schematic representation of the feature analysed. (**F, G, H**) Representation of the process based on the spheroid slicing. (**F**) Cartoon of a spheroid sectioned using the microtome. (**G**) Brightfield image of a spheroid 2D section. (**H**) Binary masks of the whole spheroid and necrotic core (manually defined by expert operators), used to calculate the necrotic percentage.

the spheroid spatially covering most of the camera's field of view (FOV); (*II*) an appropriate illumination setting (*i.e.* exposure time and lamp intensity) for having foreground grey-level values unsaturated and covering the full range available (*e.g.* 256 levels in 8-bit). After that, spheroids were fixed with Formaldehyde solution 4 % (Merck KGaA, Darmstadt, Germany) for 1 h and washed with PBS then coated with 2 % of Agarose, NuSieve® Genetic Technology Grade™ (GTG, VWR International Srl, Milano, Italy) before being embedded in Paraffin 57–60 (Merck KGaA, Darmstadt, Germany). Paraffin embedding involves a dehydration phase of the samples in ethanol solutions at increasing concentrations: 70 %, 80 %, 90 %, and 100 % then in Bio Clear (Bio Optica, Milano, Italy), in paraffin at 58 °C and finally cast in histological moulds. All spheroids were sectioned at a thickness of 5 μm using a rotary Leitz Sledge Microtome 1400 (Ostfildern, Germany, Fig. 5F). Finally, histological sections were stained using Hematoxylin and Eosin staining (H&E) to visualise nuclei and cytoplasm of the single cells in the range of visible. The staining begins with two steps: removing the paraffin with Bio Clear and with a decreasing scale of ethanol EtOH 100 %, EtOH 95 %, EtOH 75 %, EtOH 50 %; hydration with distilled H_2O. Subsequently, histological staining H&E is carried out. Specifically, the slides were immersed in Hematoxylin Mayer (Histo-Line Laboratories, Pantigliate (MI), Italia) washed in source water, and then with distilled water. At that point, the slides were immersed in an Eosin (1 %) solution (Histo-Line Laboratories, Pantigliate (MI), Italia). Followed by dehydration and closure of the histological slides: dehydration consists of a passage in ethanol solutions at increasing concentrations of EtOH 75 %, EtOH 95 % EtOH 100 %, and then in Bio Clear. For the closure, Bio Mount HM (Bio Optica, Milano, Italy) was used. Next, brightfield images of slides were acquired with the inverted Nikon Eclipse TE2000-U microscope previously described (Fig. 5G). The images were analysed and the spheroid and its necrotic core were identified by two expert operators (Fig. 5H). The Images and masks of MSC 3D spheroids (generated with three different seeding densities) and 2D sections, both analysed with a brightfield microscope (10x magnification factor, 0.41 μm/pixel conversion coefficient), are available as Supplementary Material 4. Proliferative cells tend to be arranged more densely in the superficial layers of the spheroid, while in the centre of the spheroid, the cells are less dense with separate clear areas and occasionally apoptotic nuclei are noted. In addition, the surface cells are oriented so that their long axis is parallel to the circumference of the spheroid, forming a thin fascicle. Conversely, the cells in the centre of the spheroid are oriented in a random manner, with no particular relationship to each other or the surface of the spheroid [27,28]. Therefore, since the necrotic zone presents more extracellular matrix it appears lighter in H&E staining. Using Fiji's automatic contrast tool, it was possible to distinguish a higher-intensity (necrotic) zone from a lower-intensity (proliferative) zone. These differences in signal intensity allowed an approximate boundary line to be drawn to highlight the necrotic zone (Fig. 5H).

3. Results

3.1. Spheroidisation

To quantify the effect of the MSCs on the osteosarcoma spheroids formation, area and sphericity were analysed. These features were extracted from a sample of 12 spheroids among the 48 seeded for each condition. This choice was necessary because some images had spheroids outside the image border or were compromised by debris. The results of this analysis are reported in Fig. 6. It contains a sample of images representative of the whole dataset (Fig. 6A). It is clear that, while the Saos-2 are unable to form spherical aggregates, the shape of the spheroids improves when MSCs are included. The graphs show that while the area (Fig. 6B) gets increasingly smaller with the increase in the percentage of MSCs in the spheroid, the sphericity improves, reaching a plateau between 0.8 and 0.9 (Fig. 6C). This already happens when 25 % of MSCs are mixed with the cancerous cell.

Ensuring that the model was viable at the time of analysis was essential. In particular, cell viability and metabolic activity were assessed using two complementary assays: (*I*) propidium iodide (PI), which penetrates compromised cell membranes and stains dead cells; (*II*) resazurin assay, a widely used, simple, sensitive, and non-toxic method for measuring cell metabolic activity. It relies on the reduction of resazurin, a blue, non-fluorescent dye, into resorufin, a pink, fluorescent compound, by metabolically active cells. These assays were performed specifically to verify the viability of the model at the experimental endpoint.

From the confocal images obtained analysing PI and Hoechst signals (Fig. 6D), it is possible to deduce that the hybrid spheroids appear more viable than the spheroids formed from 100 % Saos-2, as they have fewer PI-positive cells. In addition, the resazurin assay confirmed that the hybrid spheroids remain metabolically active in culture. Surprisingly, a statistically significant increase in metabolic activity was observed as the percentage of Saos-2 cells within the spheroid increased. This could be due to a different metabolism of the two lines (Fig. 6E). In fact, the intrinsic power to reduce resazurin changes according to the cell types [29]. Statistical analysis was evaluated by the one-way ANOVA using the commercial Prism software (GraphPad Software, LA Jolla, CA, USA). p-values ≤ 0.0001 (****) were considered statistically significant.

3.2. Cell number

To be able to estimate the number of cells in the spheroids, it was necessary to compute the average volume of a single MSC. The analysis was performed on a sample of 5 cells, the resulting volumes are presented in Table 1. The final volume evaluation, obtained by averaging the results, is 4352 ± 958 μm^3 (mean $\pm$ standard deviation). This value has been used as input to estimate the number of cells with *AnaSP*.

Several spheroids from each cell density group were lost during the disaggregation process, resulting in a reduced sample size. Among the remaining samples, many outliers had to be excluded from the final study due to the inaccuracy of the cell counter. Due to these factors, the number of spheroids used for the analysis was 10. *AnaSP* performs the estimation by dividing the volume of the spheroids, derived from the brightfield images by the volume of the single cell, given as input to the software. To quantify the goodness of this estimation, the numbers obtained from the cell counter were compared with the value obtained from *AnaSP*.

The obtained results for the spheroids seeded with 3000, 4000, and 5000 cells per well can be found, respectively, in Fig. 7A–C. On average, the discrepancy between the cell counter results and the ones from *AnaSP* is, respectively, 9 %, 11 %, and 7 %, which results in an overall mean discrepancy of 9 %. The tables containing the cell counting results showed in Fig. 7A–C are available as Supplementary Material 5.

3.3. Necrotic core

The necrotic percentage found with *AnaSP* was compared with the results obtained from the visual inspection of the sliced spheroids. The sample pool was composed of 3 monoculture spheroids per seeding and three negative controls with no detectable necrotic core. The absolute values resulting from the difference between the percentages obtained with the two methods were used as a comparison term (Fig. 7D). The average difference for spheroids seeded with 3000, 4000, and 5000 cells per well is 2 %, 4 %, and 4 % respectively, resulting in an overall mean difference of approximately 3 %. *AnaSP* was also capable of correctly predicting that there was no necrotic core for 2 out of the 3 negative control spheroids available. In the third one, a necrosis of 4.31 % was detected by the tool. The tables containing the cell counting results showed in Fig. 7D are available as Supplementary Material 5.
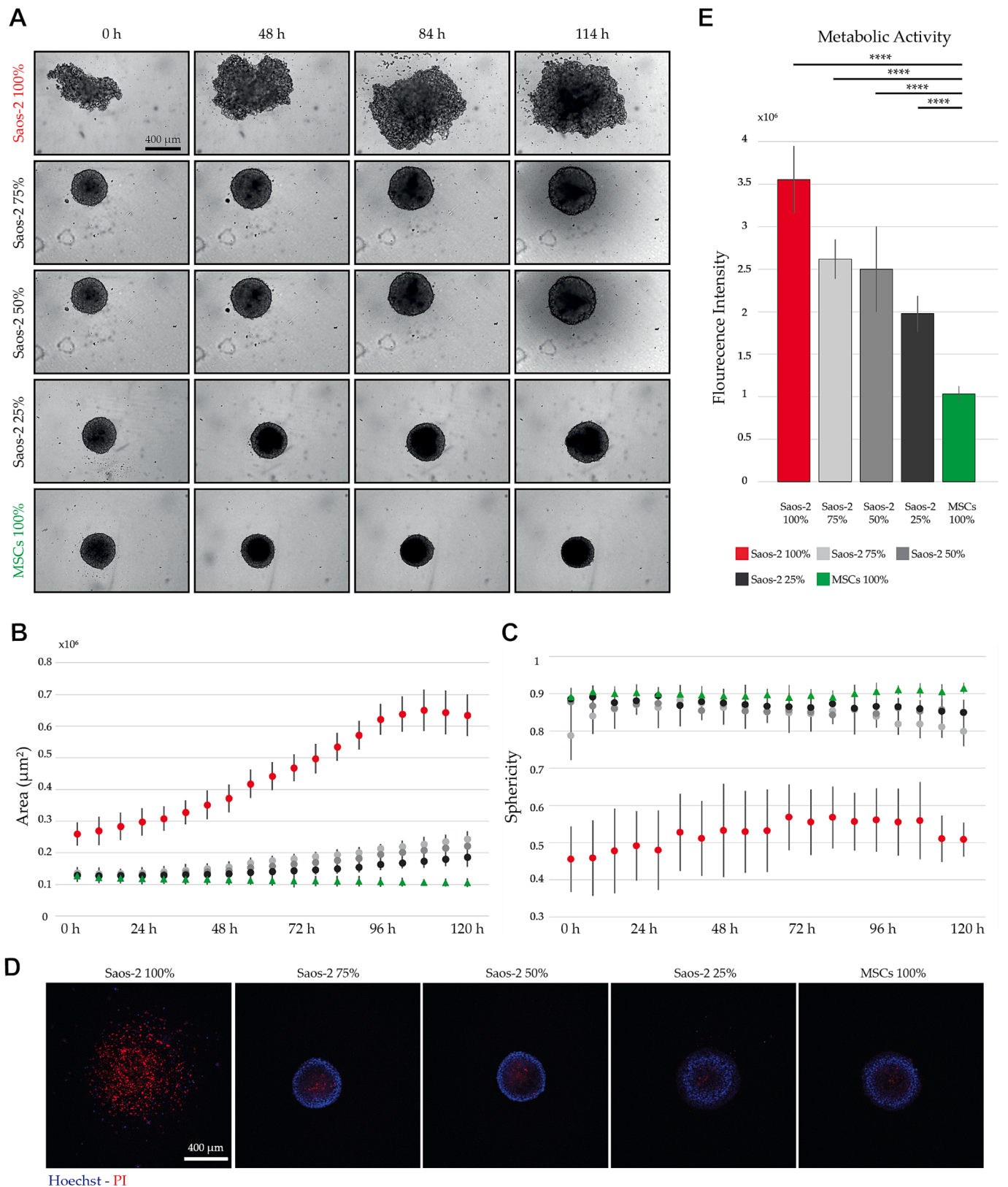
Fig. 6. Spheroidisation results. (**A**) Example images for each seeding density at four distinct time points across five different spheroid conditions (from top to bottom): 0 % MSCs and 100 % Saos-2; 25 % MSCs and 75 % Saos-2; 50 % MSCs and 50 % Saos-2; 75 % MSCs and 25 % Saos-2; 100 % MSCs and 0 % Saos-2. (**B**) Area of the spheroids in the different conditions, evaluated at 18 distinct time points. (**C**) Sphericity of the spheroids in the different conditions, assessed at the same time points as in (**B**). (**D**) Confocal images from the viability assay, performed using PI (red, showing the dead cells) and Hoechst (blue, which highlights all nuclei), in the different spheroid conditions. (**E**) Metabolic activity of the five spheroid conditions, assessed through the resazurin assay at the endpoint of the analysis. Fluorescence intensity was measured at a wavelength of 590 nm. Statistical analysis was performed using one-way ANOVA, with p-values ≤ 0.0001 (****) considered statistically significant. (For interpretation of the references to colour in this figure legend, the reader is referred to the web version of this article.)

Table 1
Volume estimation for single cells acquired with a confocal microscope.

Cell ID	Volume (μm^3)
Cell 1	5839
Cell 2	3676
Cell 3	4773
Cell 4	3917
Cell 5	3556

## 4. Discussion

4.1. Spheroidization

3D multicellular spheroids may be defined as a reliable *in vitro* tool for studying various tissues in an environment that closely mimics an *in vivo* situation [30]. With respect to other 3D models, they are preferred for the spherical shape that facilitates the manipulation and simplifies the analyses. MSCs aggregate in a nearly perfect spherical shape [31]. However, some cells like Saos-2 inherently possess a low colony-forming ability thus they do not form compact aggregates [32] if not co-cultured with other cells to enhance the compactness and sphericity of the resulting spheroids [33]. This suggests that Saos-2 cells need support to grow in a 3D model. For instance, it has been demonstrated that the formation of ECM in an MSC-Saos-2 co-culture model is driven by MSCs [15]. The enhancement in spheroid shape is likely attributed to the increased deposition of fibronectin and collagen observed in Saos-2 and

MSC co-culture models compared to Saos-2 monoculture aggregates [34]. Furthermore, the inclusion of MSCs in the culture model enhances its realism by mimicking the interactions between the tumor and stromal components found *in vivo*. Indeed, it has been demonstrated that the co-culture model displays greater resistance to anti-tumor drugs [15]. The creation and investigation of a Saos-2-MSC co-culture model provides a more complete understanding of tumour-stromal interactions, potentially offering crucial insights for the advancement of therapeutic strategies against osteosarcoma.

Our results quantitatively confirm the MSC spherification effect when added to the co-culture. The sphericity improves with the percentage of MSCs in the co-culture and remains more stable over time when more MSCs are present. However, we proved that even a small number of MSCs (*e.g.* 25 %) is sufficient to spherify the aggregates. The only behaviour worth mentioning is that after the 3rd day from seeding, the sphericity of the co-culture spheroids decreases by approximately 10 % with respect to the monoculture MSC spheroids. This could be due to the fact that Saos-2 cells divide differently than the MSCs, modifying the mixture percentage and consequently the shape of the spheroids.

4.2. Cell number

Many biological analyses are based on the number of cells composing the sample. In the case of spheroids, the most common protocol to obtain this data consists of the disaggregation of the spheroids and the use of cell counter instruments. The main limitation is that this method is highly invasive and results in the destruction of the spheroid, meaning
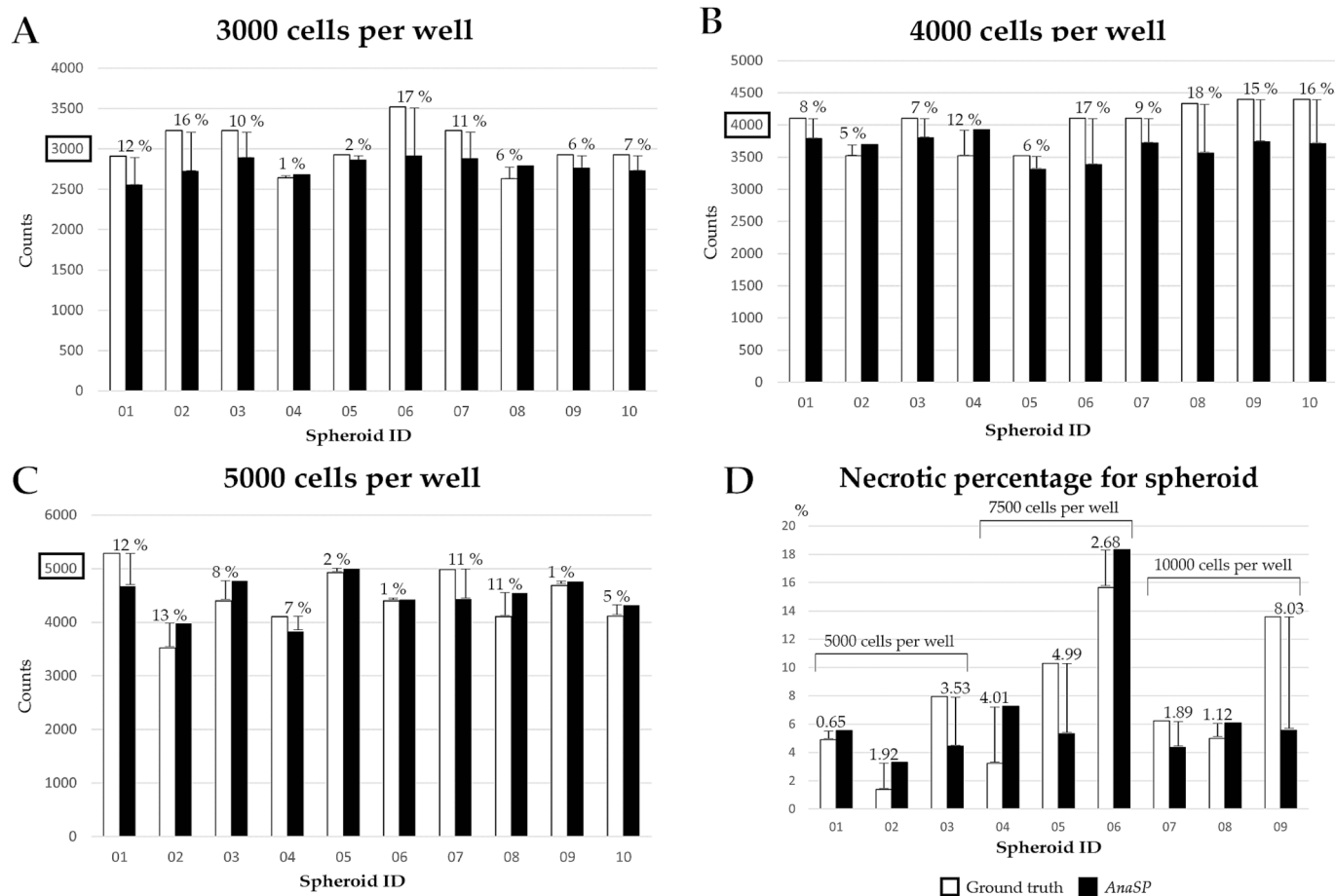
Fig. 7. Cell counting and necrotic percentage results. The discrepancy between the results of the cell counter (Ground truth) and the results from *AnaSP* are showed as bars in the histograms alongside the discrepancy percentage. (**A**) Counts for the spheroids seeded with 3000 cells per well. (**B**) Counts for the spheroids seeded with 4000 cells per well. (**C**) Counts for the spheroids seeded with 5000 cells per well. (**D**) Necrotic percentage results for the spheroids obtained with 5000 (first three columns), 7500 (middle three columns) and 10,000 (last three columns) cells per well.

no further evaluation can be done. The results of the second experiment show that the *AnaSP* software can generally estimate the number of cells in a spheroid, without destroying it, with an average discrepancy of 10 %.

To better analyse this result, it should be considered that (*a*) the "ground truth" for the cell number is typically obtained with a cell counter and often it is characterised by limited reliability due to the various passages in the protocol with non-negligible errors difficult to be quantitatively estimated. In addition, it is important to acknowledge three key limitations of *AnaSP*: (*b*) it can estimate the number of cells only for spheroids composed of a single cell type (*i.e.*, monoculture) because one of the inputs requested is the average volume of the single cells composing the spheroid and in the case of a multicultural model this can vary between the different cell lines. (*c*) Users are required to provide the pixel/unit of measurement conversion factor necessary to convert the spheroid volume from voxels to the chosen unit's cubic version (*e.g.*, cubic micrometres). This conversion factor is typically empirically estimated using micrometric beads and may yield a noisy value. (*d*) Due to the *ReViSP* algorithm used to perform the volume estimation, the more spherical the spheroid is, the more accurate the estimation of the volume and, consequently, the estimation of the number of cells will be. Nevertheless, the 10 % average discrepancy obtained shows that *AnaSP* counts the number of cells in a spheroid (without destroying the aggregate) with results comparable to invasive state-of-the-art methods [17].

4.3. Necrotic core

The obtained results support the possibility of detecting the presence of the necrotic core with a procedure not destructive for the spheroids, useful when further analyses are needed. However, several considerations should be made on the protocol used for obtaining the input data of the algorithm. In particular, it should be noted that (*a*) the necrosis detected by analysing a single slice could wrongly represent the eventual anisotropic necrosis of the spheroid. In fact, depending on the direction of the slicing and the chosen plane of analysis, a part of the necrotic core could have been neglected. On the other hand, (*b*) slicing the spheroid has a partially disaggregating effect, leaving empty regions in the final slice (Fig. 3B). The effect of this artefact is hardly reproducible when analysing the original dense spheroids. Moreover, a key limitation of the image brightness gradient approach lies in (*c*) the nature of the bright-field images, where the light does not equally penetrate along the z direction of the spheroid for different amounts of material. This affects the grey-level gradient, which is not exclusively correlated to the necrotic core. Despite these challenges, the obtained results showed an average discrepancy of 3 % in the detection of the necrotic core percentage. Additionally, *AnaSP 3.0* accurately recognised the absence of the necrotic core in 2 out of 3 of the negative controls. These results strongly support the usage of the proposed algorithm in extracting data from spheroid images without using invasive techniques.

5. Conclusions

Today, an increasing amount of data can be non-invasively extracted from spheroids, offering valuable insights into cellular behaviour and processes during drug testing and treatment evaluation.

In this work, we focused on those data that can be extracted from simple 2D brightfield images of spheroids. Besides describing *AnaSP 3.0*, an open-source software suite designed for performing radiomics with spheroids, we discussed the application of three specific features such as sphericity, volume, and image gradient, for respectively assessing spheroidization, cell number, and necrotic core extension.

In particular, the study involves experiments with monoculture and co-culture spheroids of MSCs and osteosarcoma cell lines conducted to: (*a*) understand how the presence of MSCs influences the sphericity of osteosarcoma spheroids; (*b*) estimate the number of cells composing a monoculture spheroid without destroying it; (*c*) determine presence and extension of a necrotic core within a spheroid.

The features obtainable with *AnaSP 3.0* can boost several research applications. In particular, the ability to extract data from spheroids without invasive techniques marks a significant advancement in the field of oncology and regenerative medicine. By utilising non-invasive methods, researchers can gain valuable insights into the behaviour of these 3D *in vitro* models when subjected to various drugs and treatments without losing the samples and making other subsequent analyses possible.

AnaSP 3.0 source code, standalone applications for MAC, and Windows, video tutorials, manual documentation, and sample datasets are freely available at: *https://sourceforge.net/p/anasp*.

CRediT authorship contribution statement

Mariachiara Stellato: Writing – original draft, Validation, Software, Methodology, Investigation, Formal analysis, Conceptualization. **Martyna Malgorzata Rydzyk:** Writing – original draft, Visualization, Validation, Methodology, Investigation, Formal analysis, Conceptualization. **Micaela Pannella:** Writing – review & editing, Visualization, Validation, Methodology, Investigation, Formal analysis, Conceptualization. **Francesca Rossi:** Writing – review & editing, Visualization, Validation, Methodology, Investigation, Formal analysis. **Concettina Cappadone:** Writing – review & editing, Visualization, Validation, Methodology, Investigation, Formal analysis. **Daniel Remondini:** Writing – review & editing, Supervision, Software, Resources, Funding acquisition, Data curation. **Jae-Chul Pyun:** Writing – review & editing, Supervision, Software, Resources, Funding acquisition. **Nicola Normanno:** Supervision, Software, Resources, Funding acquisition. **Toni Ibrahim:** Writing – review & editing, Resources, Conceptualization. **Gastone Castellani:** Writing – review & editing, Supervision, Software, Resources, Funding acquisition, Data curation. **Emil Malucelli:** Writing – original draft, Supervision, Resources, Project administration, Methodology, Investigation, Funding acquisition, Formal analysis, Conceptualization. **Stefano Iotti:** Writing – original draft, Visualization, Supervision, Software, Resources, Project administration, Methodology, Investigation, Funding acquisition, Formal analysis, Conceptualization. **Enrico Lucarelli:** Writing – original draft, Supervision, Resources, Project administration, Methodology, Investigation, Funding acquisition, Formal analysis, Conceptualization. **Filippo Piccinini:** Writing – original draft, Software, Resources, Project administration, Methodology, Investigation, Funding acquisition, Formal analysis, Data curation, Conceptualization.

Funding

Declaration of competing interest

The authors declare that they have no known competing financial interests or personal relationships that could have appeared to influence the work reported in this paper.

Data availability

The data presented in this study are available as supplementary Materials or at: *https://sourceforge.net/p/anasp*.

References

[1] A. Peirsman, E. Blondeel, T. Ahmed, J. Anckaert, D. Audenaert, T. Boterberg, K. Buzas, N. Carragher, G. Castellani, F. Castro, V. Dangles-Marie, J. Dawson, P. De Tullio, E. De Vlieghere, S. Dedeyne, H. Depypere, A. Diosdi, R.I. Dmitriev, H. Dolznig, O. De Wever, MISpheroID: a knowledgebase and transparency tool for minimum information in spheroid identity, Nat. Methods 18 (11) (2021) 1294–1303, https://doi.org/10.1038/s41592-021-01291-4.
[2] F. Piccinini, A. Tesei, A. Bevilacqua, Single-image based methods used for non-invasive volume estimation of cancer spheroids: a practical assessing approach based on entry-level equipment, Comput. Methods Programs Biomed. 135 (2016) 51–60, https://doi.org/10.1016/j.cmpb.2016.07.024.
[3] N. Carragher, F. Piccinini, A. Tesei Jr, O. J. T., Bickle, M., & Horvath, P., Drug Discovery. Concerns, challenges and promises of high-content analysis of 3D cellular models, Nat. Rev. 17 (8) (2018) 606, https://doi.org/10.1038/nrd.2018.99.
[4] K.H. Griffin, S.W. Fok, J. Kent Leach, Strategies to capitalize on cell spheroid therapeutic potential for tissue repair and disease modeling. Npj, Regen. Med. 7 (1) (2022), https://doi.org/10.1038/s41536-022-00266-z.
[5] F. Piccinini, AnaSP: A software suite for automatic image analysis of multicellular spheroids, Comput. Methods Programs Biomed. 119 (1) (2015) 43–52, https://doi.org/10.1016/j.cmpb.2015.02.006.
[6] Gutiérrez-Medina, B. Optical sectioning of unlabeled samples using bright-field microscopy. Proceedings of the National Academy of Sciences of the United States of America. 2022, 119(14). https://doi.org/10.1073/pnas.2122937119.
[7] E.C. Costa, D.N. Silva, A.F. Moreira, I.J. Correia, Optical clearing methods: An overview of the techniques used for the imaging of 3D spheroids, Biotechnol. Bioeng. 116 (10) (2019) 2742–2763, https://doi.org/10.1002/bit.27105.
[8] M.E. Mayerhoefer, A. Materka, G. Langs, I. Häggström, P. Szczypiński, P. Gibbs, G. Cook, Introduction to radiomics, J. Nucl. Med. 61 (4) (2020) 488–495, https://doi.org/10.2967/jnumed.118.222893.
[9] V. Härmä, H.-P. Schukov, A. Happonen, I. Ahonen, J. Virtanen, H. Siitari, M. Åkerfelt, J. Lötjönen, M. Nees, Quantification of dynamic morphological drug responses in 3D organotypic cell cultures by automated image analysis, PLoS One 9 (5) (2014) e96426.
[10] Moriconi, C., Palmieri, V., Di Santo, R., Tornillo, G., Papi, M., Pilkington, G., De Spirito, M., & Gumbleton, M. NSIDIA: A FIJI macro delivering high-throughput and high-content spheroid invasion analysis. Biotechnology Journal. I2017, 12(10). https://doi.org/10.1002/biot.201700140.
[11] M.T. Hoque, L.C.E. Windus, C.J. Lovitt, V.M. Avery, PCaAnalyser: A 2D-image analysis based module for effective determination of prostate cancer progression in 3D culture, PLoS One 8 (11) (2013) e79865.
[12] D. Lacalle, H.A. Castro-Abril, T. Randelovic, C. Domínguez, J. Heras, E. Mata, G. Mata, Y. Méndez, V. Pascual, I. Ochoa, SpheroidJ: An open-source set of tools for spheroid segmentation, Comput. Methods Programs Biomed. 200 (105837) (2021) 105837, https://doi.org/10.1016/j.cmpb.2020.105837.
[13] W. Chen, C. Wong, E. Vosburgh, A.J. Levine, D.J. Foran, E.Y. Xu, High-throughput image analysis of tumor spheroids: A user-friendly software application to measure the size of spheroids automatically and accurately, Journal of Visualized Experiments: Jove. 89 (2014), https://doi.org/10.3791/51639.
[14] Y. Hou, J. Konen, D.J. Brat, A.I. Marcus, L.A.D. Cooper, A software tool for spatial-temporal quantification of tumor spheroid dynamics, Sci. Rep. 8 (1) (2018), https://doi.org/10.1038/s41598-018-25337-4.
[15] F.E. Freeman, R. Burdis, O.R. Mahon, D.J. Kelly, N. Artzi, A spheroid model of early and late-stage osteosarcoma mimicking the divergent relationship between tumor elimination and bone regeneration, Adv. Healthc. Mater. 11 (7) (2022), https://doi.org/10.1002/adhm.202101296.

[16] F.L. Meyskens Jr, S.P. Thomson, T.E. Moon, Quantitation of the number of cells within tumor colonies in semisolid medium and their growth as oblate spheroids, Cancer Res. 44 (1) (1984) 271–277. https://pubmed.ncbi.nlm.nih.gov/6690038/.
[17] F. Piccinini, A. Tesei, C. Arienti, A. Bevilacqua, Cell counting and viability assessment of 2D and 3D cell cultures: Expected reliability of the trypan blue assay, Biol. Proced. Online 19 (1) (2017), https://doi.org/10.1186/s12575-017-0056-3.
[18] J. Lee, Y. Kim, J. Lim, H.-I. Jung, G. Castellani, F. Piccinini, B. Kwak, Optimization of tumor spheroid preparation and morphological analysis for drug evaluation, BioChip J. 18 (1) (2024) 160–169, https://doi.org/10.1007/s13206-024-00143-5.
[19] F. Piccinini, A. Peirsman, M. Stellato, J.-C. Pyun, M.M. Tumedei, M. Tazzari, O. de Wever, A. Tesei, G. Martinelli, G. Castellani, Deep learning-based tool for morphotypic analysis of 3d multicellular spheroids, Journal of Mechanics in Medicine and Biology. 23 (06) (2023), https://doi.org/10.1142/s0219519423400341.
[20] F. Piccinini, A. Tesei, C. Arienti, A. Bevilacqua, Cancer multicellular spheroids: Volume assessment from a single 2D projection, Comput. Methods Programs Biomed. 118 (2) (2015) 95–106, https://doi.org/10.1016/j.cmpb.2014.12.003.
[21] J.M. Kelm, N.E. Timmins, C.J. Brown, M. Fussenegger, L.K. Nielsen, Method for generation of homogeneous multicellular tumor spheroids applicable to a wide variety of cell types, Biotechnol. Bioeng. 83 (2) (2003) 173–180, https://analyticalsciencejournals.onlinelibrary.wiley.com/doi/pdf/10.1002/bit.10655.
[22] M. Pierini, C. Di Bella, B. Dozza, T. Frisoni, E. Martella, C. Bellotti, D. Remondini, E. Lucarelli, S. Giannini, D. Donati, American Volume. The posterior iliac crest outperforms the anterior iliac crest when obtaining mesenchymal stem cells from bone marrow. The Journal of Bone and Joint, Surgery 95 (12) (2013) 1101–1107, https://doi.org/10.2106/jbjs.l.00429.
[23] S. Lenna, C. Bellotti, S. Duchi, E. Martella, M. Columbaro, B. Dozza, M. Ballestri, A. Guerrini, G. Sotgiu, T. Frisoni, L. Cevolani, G. Varchi, M. Ferrari, D.M. Donati, E. Lucarelli, Mesenchymal stromal cells mediated delivery of photoactive nanoparticles inhibits osteosarcoma growth in vitro and in a murine in vivo ectopic model, Journal of Experimental & Clinical Cancer Research: CR. 39 (1) (2020), https://doi.org/10.1186/s13046-020-01548-4.
[24] E. Martella, B. Dozza, C. Ferroni, C. Bellotti, C. Osuru Obeyok, M. Tubertini, A. Guerrini, M. Ballestri, M. Columbaro, I. Manet, M. Gambarotti, L. Martini, M. Fini, L. Cevolani, D.M. Donati, E. Lucarelli, G. Varchi, S. Duchi, Numbers matter: The role of cell dose in the treatment of osteosarcoma using mesenchymal stromal cells as cellular vehicles, Advanced Therapeutics. 6 (10) (2023), https://doi.org/10.1002/adtp.202300045.
[25] T. Collins, Image J for microscopy, J. Biotechniques. 43 (1S) (2007) S25–S30, https://doi.org/10.2144/000112517.
[26] F. Piccinini, A. Tesei, M. Zanoni, A. Bevilacqua, ReViMS: Software tool for estimating the volumes of 3-D multicellular spheroids imaged using a light sheet fluorescence microscope, Biotechniques 63 (5) (2017) 227–229, https://doi.org/10.2144/000114609.
[27] S. Dini, B.J. Binder, S.C. Fischer, C. Mattheyer, A. Schmitz, E.H.K. Stelzer, N. G. Bean, J.E.F. Green, Identifying the necrotic zone boundary in tumour spheroids with pair-correlation functions, J. R. Soc. Interface 13 (123) (2016) 20160649, https://doi.org/10.1098/rsif.2016.0649.
[28] T.S. Deisboeck, M.E. Berens, A.R. Kansal, S. Torquato, A.O. Stemmer-Rachamimov, E.A. Chiocca, Pattern of self-organization in tumour systems: complex growth dynamics in a novel brain tumour spheroid model, Cell Prolif. 34 (2) (2001) 115–134, https://doi.org/10.1046/j.1365-2184.2001.00202.x.
[29] B. Vieira-da-Silva, M.A.R.B. Castanho, Resazurin reduction-based assays revisited: Guidelines for accurate reporting of relative differences on metabolic status, Molecules 28 (5) (2023) 2283, https://doi.org/10.3390/molecules28052283.
[30] F. Piccinini, I.D. Santis, A. Bevilacqua, Advances in cancer modeling: fluidic systems for increasing representativeness of large 3D multicellular spheroids, Biotechniques 65 (6) (2018) 312–314, https://doi.org/10.2144/btn-2018-0153.
[31] C. Bellotti, S. Duchi, A. Bevilacqua, E. Lucarelli, Piccinini Long term morphological characterization of mesenchymal stromal cells 3D spheroids built with a rapid method based on entry-level equipment. F, Cytotechnology 68 (6) (2016) 2479–2490, https://doi.org/10.1007/s10616-016-9969-y.
[32] S.U. Lauvrak, E. Munthe, S.H. Kresse, E.W. Stratford, H.M. Namløs, L.A. Meza-Zepeda, O. Myklebost, Functional characterisation of osteosarcoma cell lines and identification of mRNAs and miRNAs associated with aggressive cancer phenotypes, Br. J. Cancer 109 (8) (2013) 2228–2236, https://doi.org/10.1038/bjc.2013.549.
[33] Rimann, M., Regez, A., & Paasonen, L. Development of 3D osteosarcoma/fibroblast co-culture model using nanofibrillar cellulose, UPM Biomedicals, 13 October 2020, Application Note 30, 1-3. https://www.upmbiomedicals.com/resource-center/application-notes/development-of-3d-osteosarcomafibroblast-co-culture-model-using-nanofibrillar-cellulose/.
[34] M. Cortini, F. Macchi, F. Reggiani, E. Vitale, M.V. Lipreri, F. Perut, A. Ciarrocchi, N. Baldini, S. Avnet, Endogenous extracellular matrix regulates the response of osteosarcoma 3D spheroids to doxorubicin, Cancers 15 (4) (2023) 1221, https://doi.org/10.3390/cancers15041221.

Glossary

Mesenchymal stroma cells: spindle shaped plastic-adherent cells isolated from bone marrow, adipose, and other tissue sources, with multipotent differentiation capacity *in vitro*.

Morphological features: those features that describes the morphology of an object, such as the shape, structure, colour, pattern, and size.

Necrotic core: region within a multicellular spheroid where cells have died due to lack of nutrients and oxygen. This typically occurs in the center of the spheroid, as the outer

layers of cells consume the available resources, leaving the inner cells deprived.

Open Source: denote a software for which the original source code is made freely available and may be redistributed and modified.

Organoid: miniaturised and simplified version of an *in vivo* structure produced *in vitro* in three dimensions that mimics the key functional, structural, and biological complexity of that organ.

Osteosarcoma: malignant bone cancer that originates in the cells that form bones.

Radiomics: method that extracts a large number of features from medical images using data-characterisation algorithms. These features, termed radiomic features, have the potential to uncover tumoral patterns and characteristics that fail to be appreciated by the naked eye.

Segmentation: In digital image processing and computer vision, image segmentation is the process of partitioning a digital image into multiple image segments, also known as image regions or image objects.

Spheroid: scaffold-free spherical self-assembled aggregates of cancer cells. It is a 3-dimensional culture model which closely models oxygen gradients in small avascular tumors.

Spheroidisation: the process or technique by which cells aggregate to form a three-dimensional, spherical cluster known as a spheroid.